universität innsbruck

Experiment A001- Spectroscopy of the sun

Robin Hoffmann[*], Arik Bürkle[†], Valentin Ertl[‡]

June 10, 2025

Abstract

In this experiment, we analyze the spectrum of the Sun by measuring the iron lines. From these measurements, we calculate the effective surface temperature to be 5532,3(12) K*, the ratio of iron in its ground state to hydrogen to be* $4{,}69(3) \cdot 10^{-4}$*, and illustrate the curve of growth for the intensity of the lines.*

Contents

[*]robin.hoffmann@student.uibk.ac.at
[†]arik.buerkle@Student.uibk.ac.at
[‡]valentin.ertl@student.uibk.ac.at

1 Introduction

Solar spectroscopy, also known as solar spectrometry, is a captivating field of astronomy that focuses on the examination of the light emitted by the Sun. This area of study not only provides profound insights into the physical properties of our Sun but also plays a crucial role in exploring fundamental principles of astronomy and astrophysics. The Sun, being the nearest star to our planet Earth, offers a unique opportunity for scientists to investigate basic processes and phenomena in the universe. Spectroscopy stands out as one of the most important methods, allowing researchers to analyze the light emitted by the Sun and draw conclusions about its composition, temperature, motion, and other physical characteristics. In this context, various spectral lines in the solar spectrum are explored, arising from interactions of light with different layers and elements in the solar atmosphere. Solar spectroscopy has thus been instrumental in deepening our understanding of the structure and dynamics of our central star, serving as the foundation for numerous discoveries in astrophysics.

In this report, using the observation of solar light spectra obtained from the Echelle spectrograph at the University of Innsbruck, we determine the effective temperature and the ratio of iron to hydrogen atoms (iron abundance) in the photosphere of the Sun. The employed spectrograph and the detailed methodology for obtaining the desired values are comprehensively presented in the following sections.

2 Basics and Theory

This section discusses how the effective temperature as well as the Ratio of Iron to Hydrogen in the sun can be calculated by observing the Fe_1-lines and analysing the equivalent width of those lines.

2.1 Iron lines of the Sun

When an atom is struck by a photon, it can absorb the photon if the energy of the photon matches the energy transition of the atom. When white light is directed onto a gas, this gas absorbs photons of specific wavelengths, resulting in what is known as an absorption line. The Sun contains a small amount of iron in its outer layer, and light emitted from the Sun's interior can be absorbed by the iron atoms, causing a reduction in intensity at the corresponding wavelengths. These reductions are referred to as the iron lines of the Sun. Given that iron is a heavy atom, it possesses 205 different atomic transitions. Consequently, there are 205 iron absorption lines present in the spectrum of the Sun.

2.2 Equivalent Width

Indeed, each iron line not only absorbs light at a different wavelength but also exhibits varying effectiveness in doing so. The magnitude of absorption can be quantified through the equivalent width EW, which describes the amount of the initial light source absorbed by that specific line.

$$EW = \int \frac{I_0 - I(\lambda)}{I_0} d\lambda \tag{1}$$

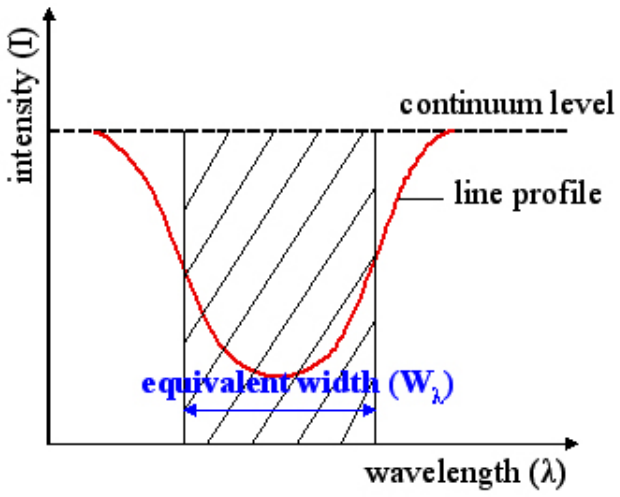

Figure 1: Equivalent width of a Gaussian [1]

The equivalent width primarily depends on two factors: the thickness of the gas layer and the likelihood of excitation. The thickness of the layer is correlated with the number of atoms in a specific excitation state; the more atoms available for excitation, the higher the likelihood of excitation. This relationship causes the equivalent width to depend on the Boltzmann distribution. As for the latter factor, the probability of absorption relies on numerous quantum calculations, which are too complex for this protocol. However, if we assume that the absorption layer is optically thin, meaning that each photon is absorbed only once, we obtain the following relation:

$$EW \propto \frac{N_{r0}}{g_{r0}} exp(\frac{\chi_i}{k_b T}) g_{rs} f_{rs} \lambda^2 \tag{2}$$

Here, r represents the ionization level of the atom, s denotes that the variable is a quantum description, g describes the degeneracy, N represents the total number of atoms, χ stands for the excitation energy of level i, T denotes the temperature, and f represents the oscillation strength.

From this ratio, by relating the number of iron atoms to the number of hydrogen atoms, we derive the equation later used:

$$log\left(\frac{EW_\lambda}{\lambda}\right) - log(\lambda \cdot g \cdot f) = -\frac{1}{k_b \cdot T} \cdot \chi + log\left(\frac{N_{Fe}}{N_H}\right) \tag{3}$$

3 Experiment setup and execution

In this section, both the functionality as well as the structure and execution of the experiment will be elucidated [2].

3.1 Setup (Échelle spectrograph)

The Échelle spectrograph was used to record the raw data in this experiment. Its structure and mode of operation are explained in more detail below. An Échelle spectrograph is an astronomical instrument designed for the analysis of stellar or celestial object spectra. An Échelle spectrograph utilizes a specialized optical arrangement to generate a high-resolution spectrum composed of numerous superimposed, parallel narrow bands. An Échelle spectrograph consists of the following components:

1. Optical Arrangement: Entrance slit and collimator: Light from the light source (e.g., a star) enters through a narrow entrance slit into the Échelle spectrograph. A collimator transforms the incident light into parallel rays.

2. Wavemaster: A Wavemaster is an optical component used to disperse light into different colors or wavelengths, often achieved through the use of gratings or prisms.

3. Échelle Grating: The pivotal component of the Échelle spectrograph is the Échelle grating, a specialized grating with high reflection or diffraction efficiency that splits light into many narrow, parallel spectral lines. These lines are referred to as "orders".[3]

4. Cross Dispersion: A second grating, known as the cross-dispersion grating, is employed to separate the various orders produced by the Échelle grating. This enables the simultaneous capture of multiple high-resolution spectra.

5. Detector: The split light is ultimately focused onto a detector, often utilizing digital detectors such as CCD cameras, which records the spectrum.

The Échelle spectrograph offers several advantages that significantly enhance the capabilities of astronomers in studying celestial objects. One key advantage lies in its remarkable high spectral resolution. Échelle spectrographs are widely recognized for their ability to provide detailed captures of fine features present in the spectra of stars and other celestial bodies. This heightened resolution allows astronomers to scrutinize intricate details, providing a deeper understanding of the composition, temperature, and other fundamental properties of these cosmic entities. Another notable advantage is the efficient utilization of data. This is achieved through the parallel arrangement of different spectral orders, a distinctive feature of Échelle spectrographs. By simultaneously recording multiple spectra, these instruments optimize data collection, streamlining the observational process. This efficiency is particularly valuable in astronomical studies, where comprehensive datasets are essential for thorough analysis and interpretation. In summary, the Échelle spectrograph not only excels in delivering high spectral resolution for detailed observations but also maximizes data utilization through its innovative design. These combined advantages empower astronomers to gain profound insights into the intricate physical characteristics of stars and other cosmic entities, contributing significantly to our understanding of the universe.[4]

3.2 Execution

3.2.1 Calibration

Besides the frames corresponding to the object of interest (the sun), several supporting frames (calibrations) need to be collected, to remove the effects introduced by the measuring process. One of these frames is the so-called Bias-Frame. In spectroscopy, a Bias-Frame is a specialized image used to rectify systematic errors, known as "bias," inherent in image data. Bias arises from electronic noise and offset voltage in a spectroscopy camera's detectors, irrespective of exposure duration or incident light. This frame is captured without exposure or with minimal exposure to isolate electronic noise and characterize detector bias stemming from factors like electronic components and temperature fluctuations.[5]
Flatfield frames are further correction images. A Flatfield-Frame in spectroscopy is an image specifically captured to correct variations in detector sensitivity across different wavelengths. These frames are taken with uniform illumination, often using a flat, evenly illuminated source, allowing for the identification and correction of pixel-to-pixel sensitivity variations in the spectroscopy system. This correction is crucial for obtaining accurate and reliable spectral data by compensating for uneven response across the detector. In summary, the Flatfield-Frame serves to normalize and enhance the quality of spectroscopic observations by mitigating detector sensitivity discrepancies.[6]
Last but not least we need Wavelength Calibration Lamps as calibration for this experiment. Wavelength calibration lamps are light sources emitting well-defined emission lines, serving to create a calibration spectrum for precise wavelength mapping in spectrometers or spectrographs. Characterized by known emission lines, these lamps facilitate accurate calibration by comparing measured positions of lines with their known wavelengths. Common types include mercury vapor, neon, and argon lamps, each generating characteristic lines. Regular use of calibration lamps ensures instrument accuracy and stability during experimental measurements in diverse fields such as astronomy, chemistry, biology, and materials science. In essence, these lamps are indispensable tools that enhance the reliability and precision of wavelength measurements in spectroscopic applications.
All the calibration images just described had to be recorded in order to obtain the best possible corrected data for the evaluation.[2]

3.2.2 Extraction of the Stellar Spectrum

Once the images undergo bias subtraction, flatfield correction, and wavelength calibration, our goal is to extract the stellar spectrum by defining regions of interest around the stellar signal on the detector and summing the flux within these regions to produce a one-dimensional spectrum. Subsequently, background subtraction is performed to eliminate contamination from sky background or nearby stars, followed by normalizing the stellar spectrum by dividing it by a suitable continuum reference to remove flux level variations. This normalization ensures accurate representation of relative intensities of spectral features and facilitates determination of line equivalent widths. [2]

4 Resulting Data

In this section, we present the resulting data obtained from our measurements and depict them in graphical representations. Employing linear regression analyses on the datasets, we derive the effective temperature of the Sun, along with the ratio of iron to hydrogen in the outer layer of the Sun.

4.1 Data Analysis

After conducting the experiment, the data from the spectrograph undergoes a cleansing process to rectify systematic errors inherent in the equipment and is calibrated as described in Section 3.2.1. From the resulting dataset, we ascertain the equivalent width of various iron lines by fitting the spectrum with a Gaussian curve and computing the area beneath the curve, as indicated in Equation 1. Certain lines may overlap with others, rendering the Gaussian fit nonsensical; thus, data points with indeterminate peaks are eliminated. Furthermore, any data exhibiting illogical measurements of wavelength are discarded.
To derive the effective temperature as well as the ratio of iron to hydrogen, we conduct linear regressions of the data, as described in Equation 3. A prerequisite for a reliable linear fit is the utilization of optically thin lines where each photon is absorbed only once. Consequently, data points with equivalent widths exceeding 0,1 Å are excluded.

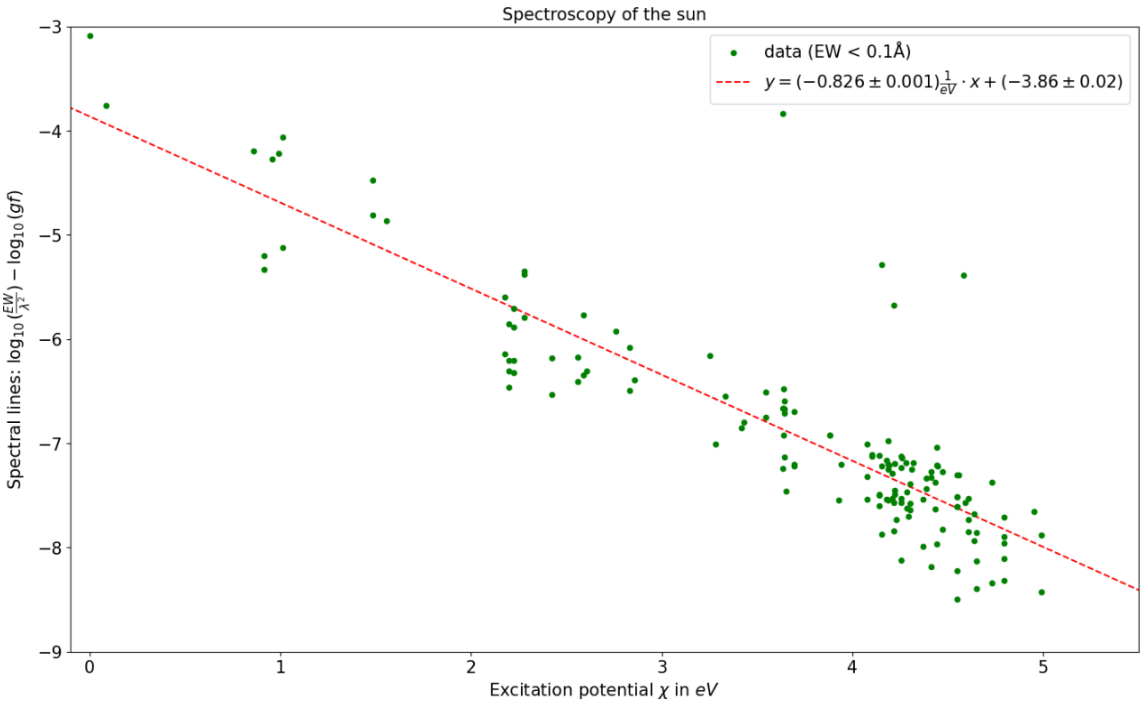

Figure 2: The diagram illustrates the spectral lines plotted against the excitation potential χ for all datasets where the equivalent width EW is less than 0.1 Å. Subsequently, a linear regression analysis was conducted utilizing the function: $y = -0{,}826(1)\,\mathrm{eV}^{-1} \cdot x - 3{,}86(2)$.

From this regression (Figure 2), we calculated that the effective temperature of the Sun is $T = 6101(10)\,\mathrm{K}$ and an iron to hydrogen ratio of $N_{Fe}/N_H = 1{,}37(7) \cdot 10^{-4}$.
With these values, it is possible to plot the Standard Curve of Growth for the entire dataset, as illustrated in Figure 3. As observed, our data aligns well with the predicted Standard Curve of

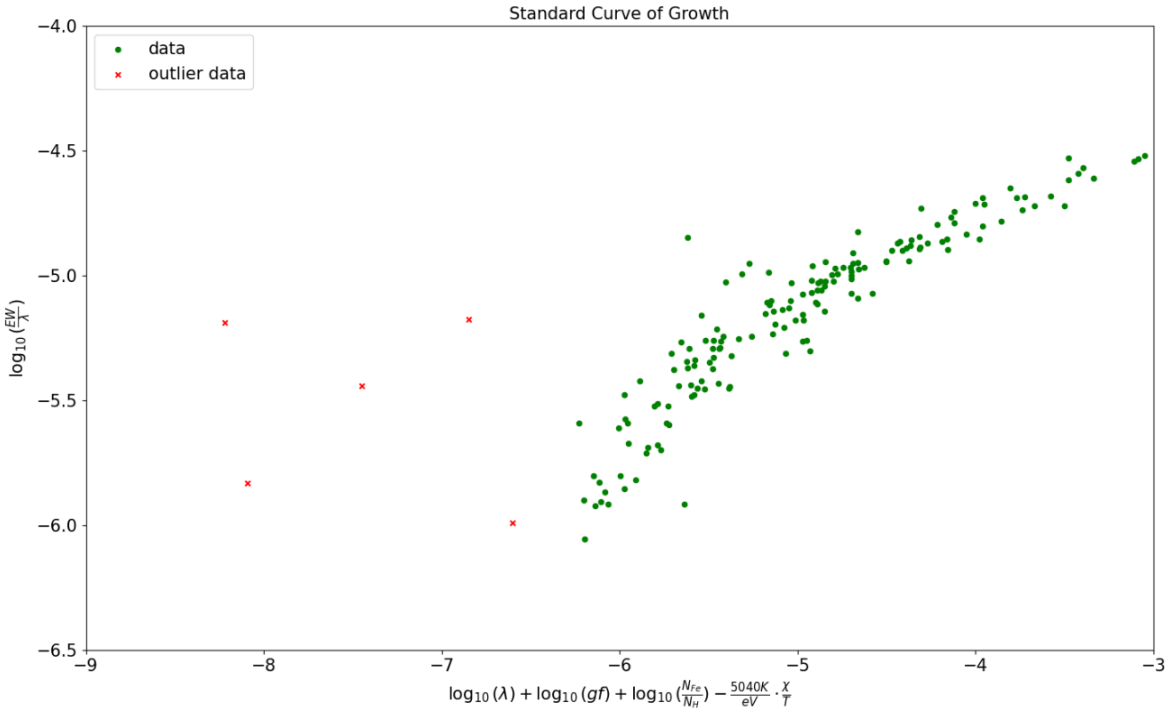

Figure 3: The diagram illustrates the Standard Curve of Growth for the entire dataset. Additionally, outlier data, which is not further considered based on this diagram, is depicted in red.

Growth. Initially, the data follows a linear trajectory with a slope of near to 45°. Subsequently, the curve flattens out, consistent with expectations from the Standard Curve of Growth. Several data points, highlighted in red, exhibit clear outlier behavior, likely representing lines overlapping with different lines. These points will be excluded and eliminated from the dataset for subsequent analysis.
The Standard Curve of Growth is then partitioned into two segments, as depicted in Figure 4. The first segment comprises optical thin lines of the spectrum, which should adhere to the 45° slope. The second segment encompasses all points with a value of $x > -5.25$, representing optical thick lines where a photon can interact multiple times with an atom.

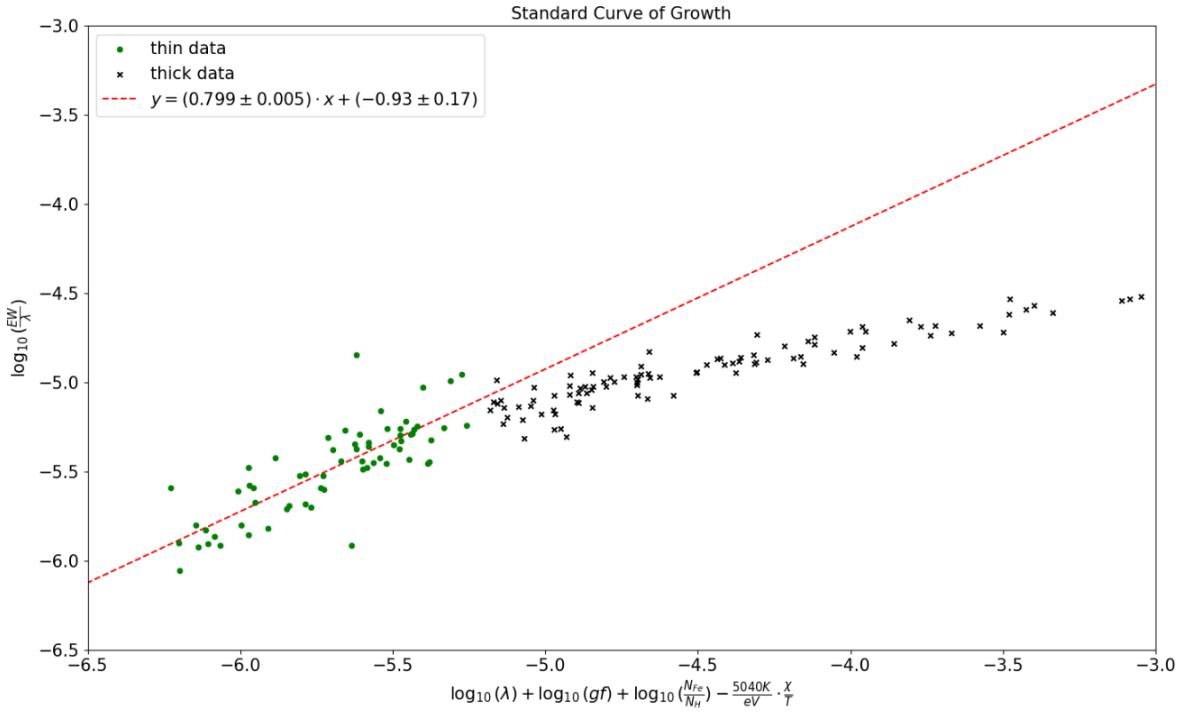

Figure 4: The diagram depicts the Standard Curve of Growth and divides the remaining dataset into two groups. Data points corresponding to the thick lines are represented by black crosses, while the green dots represent data points associated with the thin lines. Additionally, a linear regression is applied to the latter, represented by the following function: $y = 0{,}799(5) \cdot x - 0{,}93(17)$.

From the diagram in Figure 4, it is evident that the thin data follows a much steeper curve compared to the thick data. However, the curve does not exhibit a slope of 45°, which would imply a gradient of 1, instead it has a gradient of 0,799(5). This deviation could be attributed to the inclusion of optical thick lines in the dataset used to calculate the temperature as well as the iron to hydrogen ratio.

By recalculating using the new optical thin dataset, the following regression is obtained, as described in Equation 3: From the linear fit in Figure 5, we derive the new effective temperature of the Sun to be $T = 5532{,}3(12)\,\mathrm{K}$ and an iron to hydrogen ratio of $N_{Fe}/N_H = 4{,}69(3) \cdot 10^{-4}$. With these new values obtained solely from thin lines, we construct the Standard Curve of Growth again, as shown in Figure 6. This curve aligns even more closely with the expected curve than the initial Standard Curve of Growth (Figure 4) . Here, we observe a gradient of 0,872(4), which is even closer to the expected gradient of 1. Once more, it is evident that at a certain point, the lines become saturated and deviate from the straight line.

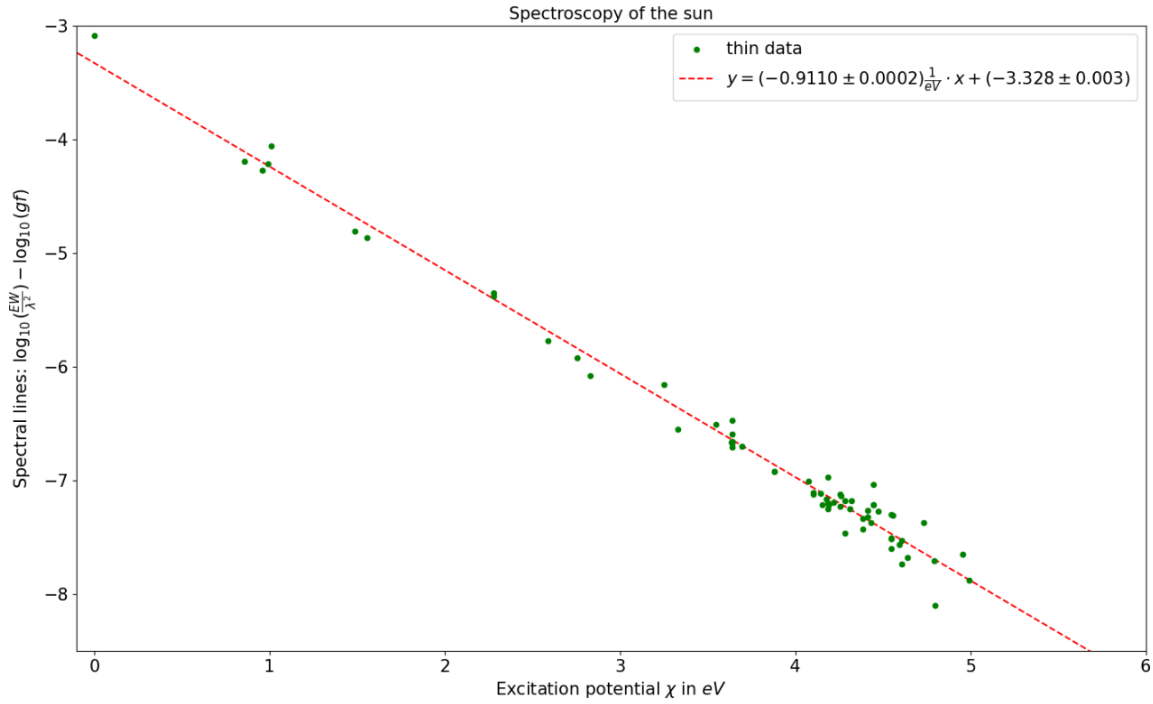

Figure 5: The diagram illustrates the spectral lines plotted against the excitation potential χ for the datasets of the thin lines (marked green in Figure 4). Subsequently, a linear regression analysis was conducted utilizing the function: $y = -0{,}9110(2)\,\mathrm{eV}^{-1} \cdot x - 3.328(3)$.

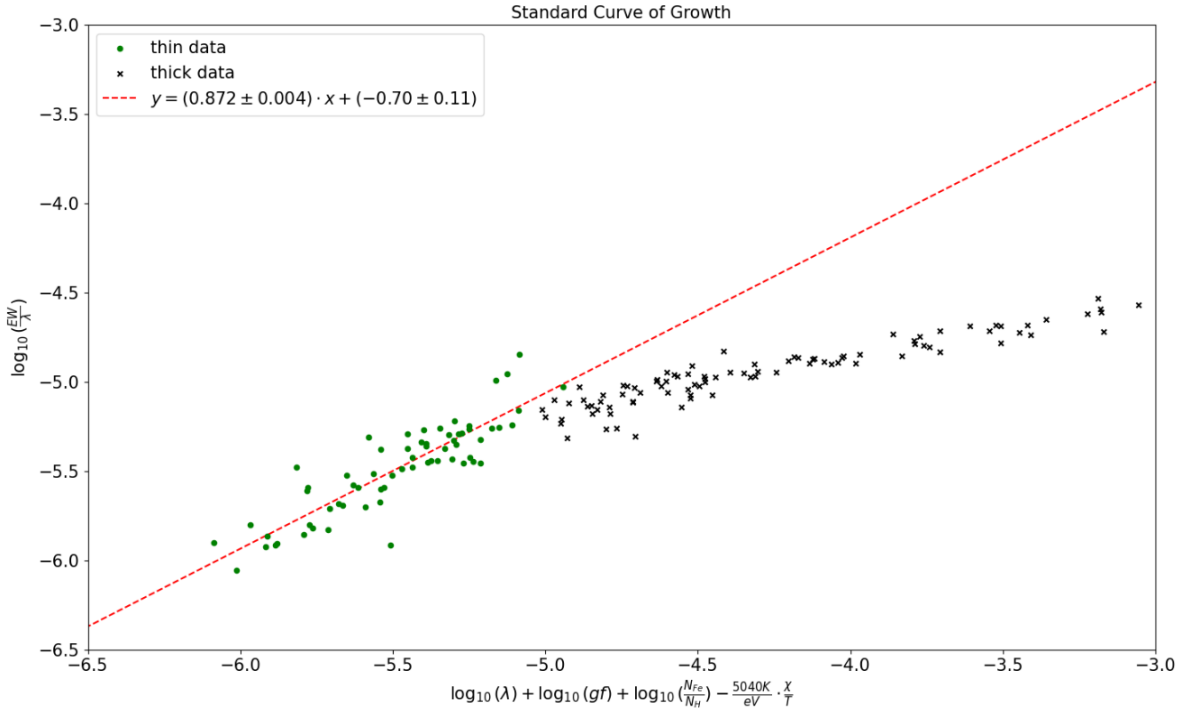

Figure 6: The diagram illustrates the Standard Curve of Growth for the previously partitioned dataset, considering the effective temperature and metallicity calculated from the linear regression in Figure 5. Once more, data points corresponding to the thick lines are denoted by black crosses, while the green dots represent data points associated with the thin lines. The linear regressions for the dataset of the thin lines, is represented by the following function: $y = 0{,}872(4) \cdot x - 0.70(11)$.

4.2 Systematic errors in the experiment

During the execution of the experiment, several errors were not accounted for, resulting in deviations from the literature results of the quantities calculated in the experiment.
The primary issue with the experiment lies in the omission of measurement errors. Although efforts were made to minimize errors by thoroughly calibrating the instrument, various factors affecting the measurement were inevitably present. Identifying these errors would necessitate multiple measurements and averaging to obtain proper error estimates for the data. Consequently, errors in the equivalent width from the Gaussian fit were not incorporated. Additionally, determining an exact cutoff between thin and thick lines was challenging; the cutoff point was merely estimated, and with more measurements, a clearer delineation could be established.
Another limitation is that only neutral iron lines of the Sun were measured. For a more accurate calculation of the effective temperature of the Sun, the entire spectrum of the Sun should be analyzed. However, conducting such a measurement would be excessively time-consuming and intensive for the purposes of this experiment. Moreover, the measurement of only neutral iron leads to an incomplete detection of all iron species, causing the iron to hydrogen ratio to shift.
Furthermore, a significant challenge in measuring the iron to hydrogen ratio lies in the fact that it ideally encompasses the ratio for the entire star. However, in this experiment, it is only feasible to measure this ratio in the outer shell of the star due to the inherent nature of our observations. As a result of the star's construction, the ratio of iron in the outer shell is much larger than that inside, resulting in a discrepancy in our measurement.

5 Discussion of Results

In this experiment, the solar spectrum was analyzed, revealing the effective temperature of the Sun to be 5532,3(12) K and the iron to hydrogen ratio of the outer shell of the Sun to be $4{,}69(3) \cdot 10^{-4}$. Both values deviate significantly from their respective literature values of 5772 K [7] and $3{,}2 \cdot 10^{-5}$ [8]. However, these deviations can reasonably be explained by the accumulation of the previously discussed errors.
Furthermore, it was demonstrated that the spectral lines adhere to the Standard Curve of Growth. It was observed that thin lines exhibit a nearly linear growth with a logarithmic slope of 0,872(4), slightly deviating from the expected slope of 1. This discrepancy, as argued, also arises from systematic errors present in the experiment.
In conclusion, the solar spectrum of the Sun can indeed be utilized to derive various quantities of the star. However, for more accurate results, a much more thorough observation must be conducted to mitigate the aforementioned errors.

References

[1] Wikipedia. *Equivalent width*. Online; State: February 21, 2023. Retrieved on March 12, 2024. URL: https://en.wikipedia.org/wiki/Equivalent_width.

[2] Universität Innsbruck - Fakultät Astrophysik - Miguel A. Urbaneja. *Fortgeschrittenen-Praktikum: Experiment A1 – Spectroscopy of the Sun*. Skript; State: February 2024. Retrieved on March 12, 2024.

[3] Wikipedia. *Echelle grating*. Online; State: March 10, 2024. Retrieved on March 12, 2024. URL: https://en.wikipedia.org/wiki/Echelle_grating.

[4] Universität Tübingen - Institut für Astronomie und Astrophysik. *Das Echelle-Spektrometer*. Online; State: April 20, 2021. Retrieved on March 12, 2024. URL: https://uni-tuebingen.de/fakultaeten/mathematisch-naturwissenschaftliche-fakultaet/fachbereiche/physik/institute/astronomie-und-astrophysik/astronomie-hea/forschung/abgeschlossene-projekte/orfeus/echelle-spektrometer/.

[5] Practical Astrophotography. *A brief guide to calibration frames*. Online; State: June 28, 2018. Retrieved on March 12, 2024. URL: https://practicalastrophotography.com/a-brief-guide-to-calibration-frames/.

[6] Wikipedia. *Flat-field correction*. Online; State: September 14, 2023. Retrieved on March 12, 2024. URL: https://en.wikipedia.org/wiki/Flat-field_correction.

[7] Wikipedia. *Sonne*. Online; State: February 10, 2024. Retrieved on March 12, 2024. URL: https://de.wikipedia.org/wiki/Sonne.

[8] Wikipedia. *Metallizität*. Online; State: March 7, 2024. Retrieved on March 12, 2024. URL: https://de.wikipedia.org/wiki/Metallizit%C3%A4t.

Explination

Hereby, we confirm that the present report was written independently and all necessary sources and references have been provided.

Arik Bürkle	12.03.2024
Student 1	Datum
Robin Hoffmann	12.03.2024
Student 2	Datum
Valentin Ertl	12.03.2024
Student 3	Datum